

Self-propelled Droplets from Bioinspired Directional Microstructured Surfaces

Corey M. Kruse¹, Isra Somanas¹, Evan Brown¹, Troy Anderson², Chris Wilson², Craig Zuhlke²,
Dennis Alexander², George Gogos¹, Sidy Ndao*¹

¹University of Nebraska – Lincoln, Mechanical and Materials Engineering, Lincoln, NE 68588

²University of Nebraska – Lincoln, Electrical Engineering, Lincoln, NE 68588

ABSTRACT

Directional and ratchet like functionalized surfaces can induce liquid transport without the use of an external force. In this paper, we investigate the motion of liquid droplets near the Leidenfrost temperature on functionalized bioinspired asymmetric microstructured surfaces. The surfaces, which we have named “fish scale” microstructures, display unidirectional properties. The surfaces are fabricated on stainless steel through the use of a femtosecond laser-assisted process. Through this femtosecond process, mound-like microstructures on the surface are formed through a combination of material ablation, fluid flow, and material redeposition. In order to achieve the asymmetry of the structures and geometry, the femtosecond laser is focused at an angle with respect to the sample surface to give the microstructures a fish scale or ratchet like appearance. Two surfaces with 45° and 80° microstructures were fabricated. Droplet experiments were carried out to characterize the directional and self-propelling properties of the surfaces. It was found that the velocity of the liquid droplet deposited on such heated surfaces is a function of surface temperature. It was found that the maximum velocities were 12.5 and 17.8 cm/s for the 80° and 45° samples, respectively. It was also found that the droplet motion direction is opposite of that for a surface with conventional ratchet microstructures. A new mechanism for a self-propelled droplet on an asymmetric three dimensional self-organized microstructured surfaces has been proposed.

KEY WORDS: New Materials, Thermophysical Properties, Boiling and Evaporation, Droplet Motion, Directional Surfaces, Femtosecond Laser

1. INTRODUCTION

Controlling and moving liquid droplets is very important in many applications such as microfluidic, ink-jet printing, lab-on-a-chip, droplet microfluidics and fuel injection for combustion applications. Fluids are conventionally moved through the application of an asymmetric potential like a pressure gradient (pumps, compressors, etc.). In small applications it is typically difficult to use a conventional method for moving a fluid. It has been shown that it is possible to move droplets without conventional means. Liquid droplets can be moved and controlled with an asymmetric potential created by varying surface tensions from chemical and thermal gradients [1–6] as well as with the use of magnetic control [7]. These methods have the disadvantage of requiring some sort of power source as well as typically being limited to a small working distance.

When a liquid droplet is placed on a heated surface at a temperature slightly above the saturation temperature of the liquid, the droplet evaporates in a very short amount of time as a result of very efficient nucleate boiling. As the surface temperature and heat flux are increased, vapor pockets begin to form between the droplet and surface. These vapor pockets gradually insulate the heated surface. At much higher temperatures these vapor pockets eventually form a stable vapor film between the droplet and the heated surface. This vapor film efficiently insulates the droplet and dramatically increases the droplet evaporation time. The

*Corresponding Author: sndao2@unl.edu

temperature at which this phenomenon occurs is referred to as the Leidenfrost temperature [8]. A droplet in this state has the unique characteristic of being supported in a nearly frictionless state by its vapor layer [9–11]

Since droplets in the Leidenfrost state are in a nearly frictionless state, it takes very little force to sustain their motion. This characteristic of droplets in the Leidenfrost state has been exploited in self-propelled droplets on ratchet surfaces [12–18]. These types of surface structures have been shown to be very effective at moving droplets across a substrate and over a relatively long distance with considerably high speeds. Depending on the surface temperature, the surface structure profile, and the droplet size, the droplet speed can be on the order of 5–40 cm/s [12–18].

In our current work we have been able to show very similar self-propelled Leidenfrost droplet results with a three dimensional self-organized microstructured surfaces. In our experiments, functionalized bioinspired asymmetric microstructured surfaces are created with the use of a femtosecond laser process on stainless steel. These microstructures, which we refer to as “fish scale” microstructures, exhibit unidirectional surface properties. The structures are referred to as fish scale structures because they consist of mound like structures that overlap each other in a self-organized pattern. The angle at which the scales overlap was varied between samples. The direction of droplet motion on our surfaces is opposite to that reported for ratchet surfaces.

2. Experimental Procedures

2.1 Laser Manufacturing Multiscale surfaces (surfaces with features on both the micrometer and nanometer scales) that range from superhydrophobic to superhydrophilic are commonly fabricated for functionalized surfaces [19–24]. Indeed, such surfaces are considered to be biologically inspired as they often mimic the surfaces of plant leaves; one iconic example is the superhydrophobic lotus leaf which exhibits self-cleaning properties due in part to its multiscale surface features [25,26]. For such structured surfaces, the relative sizes of both micrometer and nanometer scale structures are critical for the control of not only the contact angle, but also the adhesion and wetting state [26–28].

Femtosecond laser surface processing (FLSP) is rapidly emerging as a powerful and dynamic method for the fabrication of biologically inspired multiscale surface structures. Using this process, surfaces generally consist of self-organized, quasi-periodic micrometer-scale conical or mound structures that are covered in a layer of nanoparticles [28–36]. Unlike the ratchet surfaces that are formed with a conventional milling technique, these surface structures are self-organized and are formed through a complex combination of multiple growth mechanisms including laser ablation, capillary flow of laser-induced melt layers, and redeposition of ablated material.

A schematic of the FLSP setup is shown in Figure 1. The laser used in this work was a Ti:Sapphire (Spitfire, Spectra Physics) that produced ~50 fs pulses centered around 800 nm at a 1 kHz repetition rate. The laser power was controlled through a combination of a half waveplate and a polarizer. A refractive Gauss-to-top hat beam shaper (Eksma Optics, GTH-4–2.2FA) was used to generate a top hat beam with a square profile; this ensured that the laser fluence (power) on the sample was uniform. The sample was placed on a computer-controlled 3D translation stage and translated through the beam path of the laser in order to process an area larger than the laser spot size. The number of pulses incident on the sample was controlled by the translation speed of the sample. The angle of the fish scale structures was controlled by changing the incident angle of the laser.

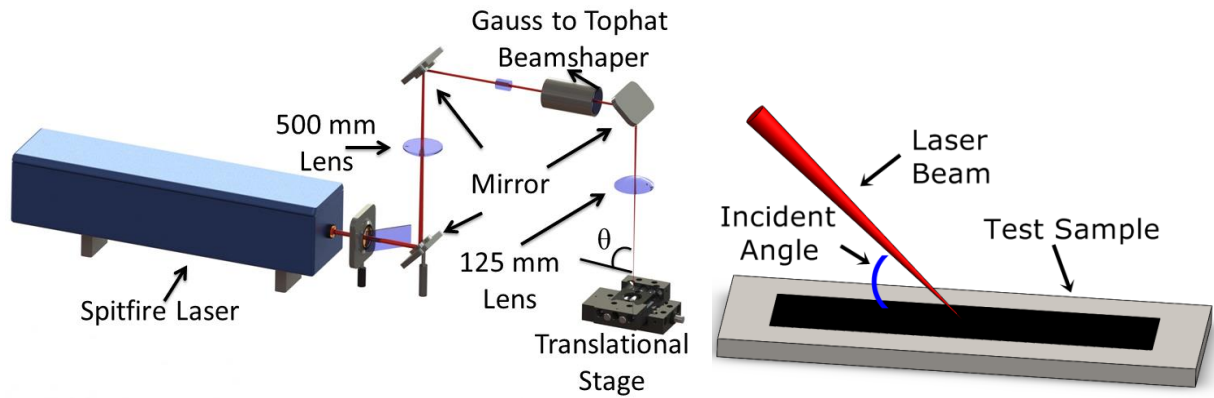


Fig. 1 Left - Schematic of the femtosecond laser surface processing (FLSP) setup, Right – enlarged view of laser beam incident angle

2.2 Tailoring Multiscale Surfaces The size and shape of self-organized surface structures fabricated via FLSP are controlled through various fabrication parameters including the laser fluence, the number of laser shots per area incident on the sample, and the composition and pressure of the atmosphere during processing. In the present study, a pair of multiscale surface morphologies was fabricated on stainless steel with a microstructure angle of 45° and 80° with respect to the horizontal and then utilized to demonstrate the ability to self-propel Leidenfrost droplets.

The fluence and shot number were chosen as control parameters as they represent two contrasting methods of controlling the total dose of laser energy transferred to a substrate. To illustrate this, consider that a given amount of laser energy can be transferred to a target substrate either through a small number of laser pulses with a large fluence or through a large number of laser pulses with a small fluence. However, the laser fluence critically impacts the laser–matter interaction mechanisms attributed to the development of multiscale structures; we recently published a shot-by-shot study of the ability of the laser fluence to influence the physical formation mechanisms of the self-organized surface structures and utilized this control to fabricate multiscale metallic surface structures that rise above the original surface[36]. Thus, control of the laser dose via a calculated selection of both the laser fluence and the number of pulses on the sample is a convenient method to produce a range of unique surface morphologies. In the present study the surface morphology was intended to remain invariant by keeping the shot and fluence combination the same for each sample while varying only the laser incident angle.

2.3 Surface Characterization A series of SEM images was used to help characterize the surfaces as well as compare the differences between their microstructures. In order to show how the microstructures overlap each other to form the fish scale pattern, SEM images were taken from the side as well as normal to the surface. SEM images were also taken with the SEM stage tilted to 45° and 80° respectively to see the variation in microstructures when looking along the microstructure direction. These images are shown in Figure 2.

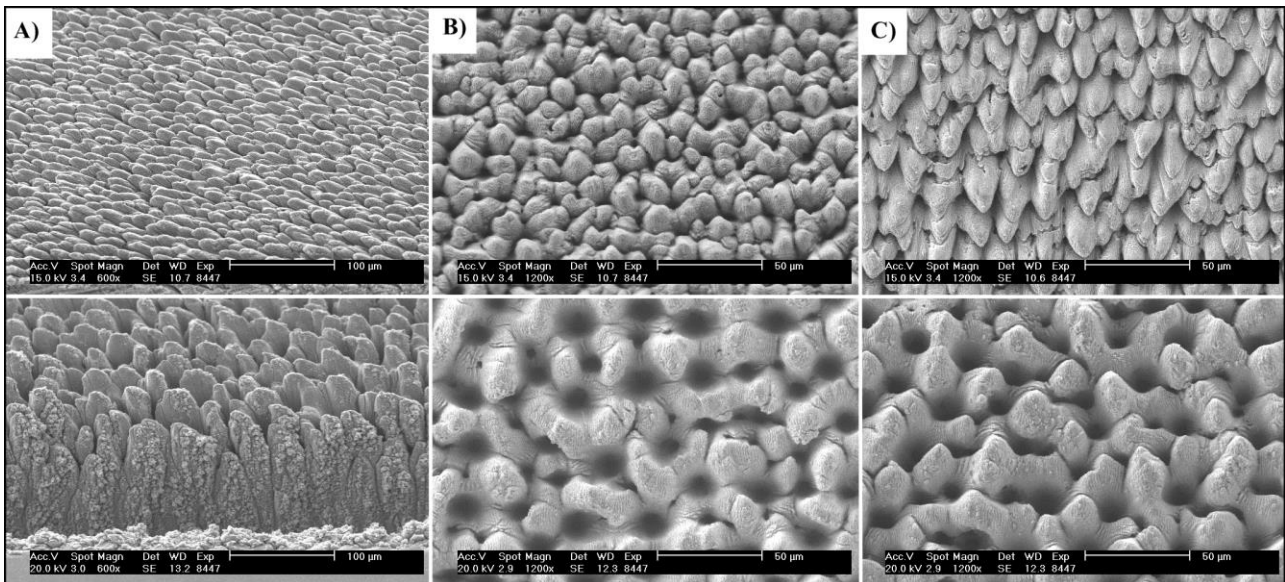


Fig. 2 SEM images of the 45° (top) and 80° (bottom): A) Looking at sides of structures (600X and 100 μm scale bar) , B) Looking along the microstructures (1200X and 50 μm scale bar), C) Looking normal to the surface (1200X and 50 μm scale bar)

Although the laser power and shot number were held the same for both samples, the two samples are not quite identical. The microstructure type of geometry appears to be nearly the same for both samples; both samples have mound like structures with round tops. The 45 degree sample microstructures appear to be shorter in height compared to the 80 degree sample and also more densely packed. The 45 degree sample has microstructures that are tilted with respect to vertical along their entire length, whereas the 80 degree sample shows a tilt only at the very tip of the microstructure. It can also be seen from the SEM images that the microstructures are formed in a self-organized fashion. The variation in the samples is due to the incident angle of the laser. When the angle of the laser is changed the amount of energy per unit area transferred to the surface also changes and thus creates a slightly different surface morphology.

2.4 Motion Experiment The experimental samples were created on a 2.5” x 1” piece of polished 316 stainless steel plate. The fish scale structure was processed to be 0.5” wide and 2” long and located in the center of the plate. The processed sample was then placed onto a copper heating block heated by five cartridge heaters. Four K-type thermocouples (Omega 5TC-GG-K-36-72) were epoxied (Omega OB-200-2) to the surface of the test sample in order to accurately determine the surface temperature. The surface temperature was monitored with the use of LabVIEW. The surface temperature was controlled through the use of a Rame-Hart precision temperature controller (Rame-Hart 100-50) and a thermocouple feedback loop. Droplet size and dispensing was controlled by a Rame-Hart computer controlled precision dropper (Rame-Hart 100-22). Droplet sizes were set to 10.5 μL during the experiment. This size was chosen because it corresponds to the droplet size that detaches from the needle by gravity. The droplets were released from the needle by gravity and were released as close to the surface as possible to limit the effects of the impact velocity. From high speed video analysis it was determined that the droplets were released from the needle with an average velocity of 8.1 cm/s. This corresponds to a weber number ($We = \frac{\rho D_0 V_0^2}{\gamma}$) of around 0.52 ($\rho=998 \text{ kg/m}^3$ and $\gamma = 73\text{mN/m}$ at room temperature). All videos were recorded with the use of a high speed camera (Photron Fastcam SA1.1), set at 250 frames per second. Figure 3 shows a schematic of the experimental setup.

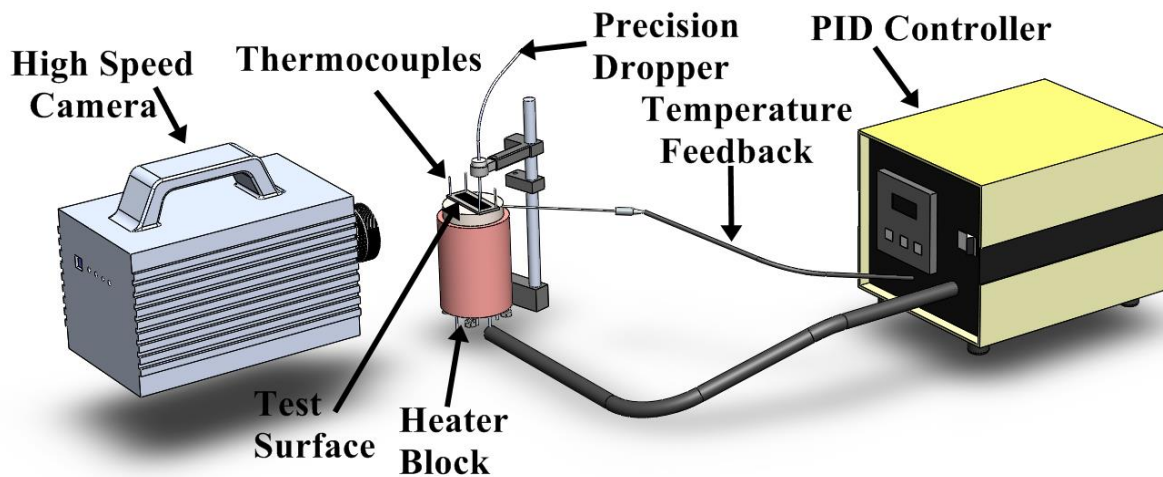


Fig. 3 Schematic of the experimental setup used for characterizing the droplet motion

Droplets were released onto the processed strip at a distance of about 0.5" from one end of the processed area (see results section). The droplet was then allowed to travel over a total distance of 1.75". The entire motion of the droplet was recorded with the high speed camera. The surface temperature of the processed strip was varied from 250 °C to 400 °C. For each temperature ten droplet velocities were recorded. The droplet velocity reported is the average velocity as the droplet transitions from the processed to unprocessed area. This velocity was calculated by the use of the high speed video. For each of the ten droplet runs, five velocities were calculated in the last 0.5" of the processed strip. These five velocities were averaged and considered to be the average speed of the droplet as it transitioned from the processed to unprocessed area. This was done for each of the ten runs at each temperature and then these ten velocities were averaged and reported as the velocity of the droplet at that specific temperature.

3. RESULTS

Figure 4 shows the data obtained from the droplet motion experiments. As can be seen from the graph there is quite a difference between the two samples. The velocity curve for the 80° sample monotonically decreases for the range of temperatures considered while the 45° sample has a maximum at around 300 °C. The 80° sample exhibits a maximum velocity of 12.5 cm/s while the 45° sample had a maximum velocity of 17.8 cm/s. Both samples exhibit a decrease in velocity as the temperature increased. This was expected, as well as reported by others [17]. It is believed that if the temperature range was expanded to lower temperatures, the 80° sample would eventually exhibit a local maximum at lower temperatures similar to the 45° sample. If the temperature range was extended to higher temperatures, the 45° sample would eventually converge to a more steady velocity like the 80° sample.

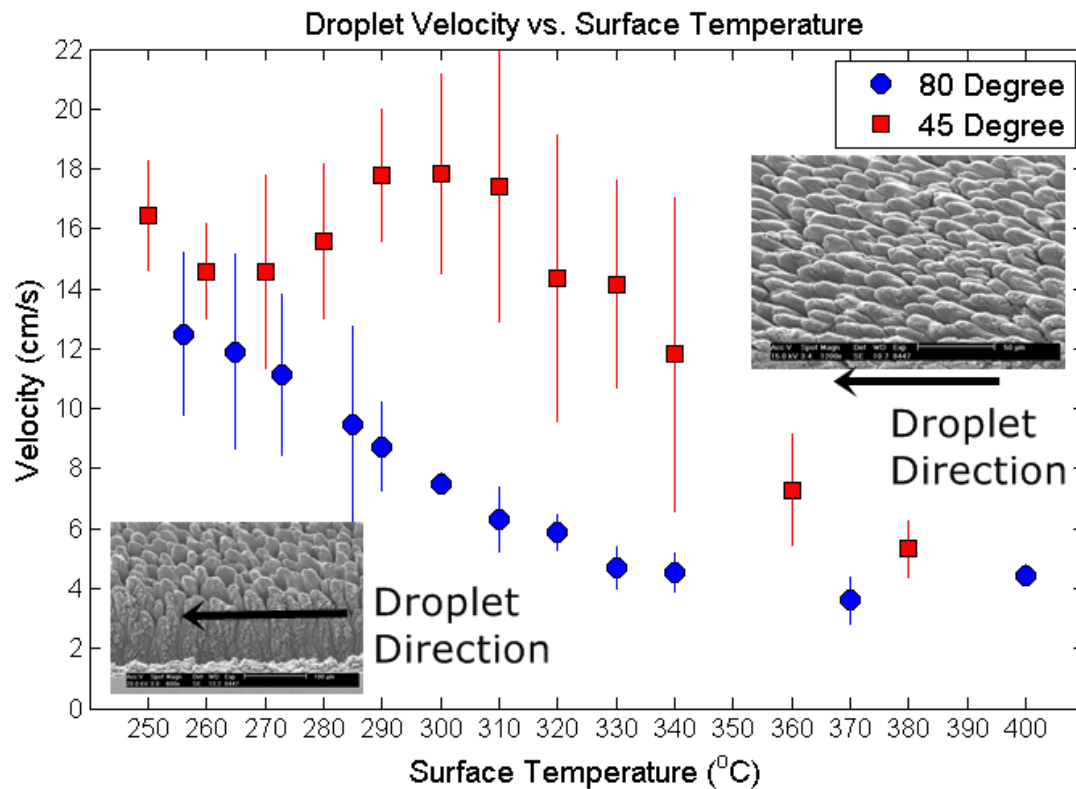


Fig. 4 Droplet velocities with respect to surface temperature for both processed samples.

It can be seen from the graph and the high speed video that there are two distinctly different mechanisms that aid to the motion of the droplet. There is a dynamic balance between the two mechanisms at play. At different temperature ranges one of the two mechanisms dominates the other. The temperature range at which one mechanism dominates is dependent on the Leidenfrost temperature of the surface [28]. At temperatures below the Leidenfrost temperature of the droplet, motion results from the directional ejection of vapor due to intermittent contact between the liquid droplet and microstructures [14,28,37,38]. When this intermittent contact happens heterogeneous boiling occurs and vapor is violently released from the droplet resulting in higher droplet velocities. At temperatures above the Leidenfrost temperature, a stable vapor film is created and thus the intermittent contact between the droplet and microstructures is less likely to happen. At these temperatures, the droplet motion is dominated by viscous stress that drags the droplet in the direction of the vapor flow. Because this mechanism is much less violent than the intermittent contact, it produces a smaller but more stable force on the droplet corresponding to slower velocities.

From figure 4 and the high speed videos, it was estimated that the Leidenfrost temperature for the 80° and 45° sample were 330 °C and 360 °C respectively. These Leidenfrost temperatures are within the expected range for surfaces created by a femtosecond laser process [28]. This was determined by a combination of the change in the graph slope, the standard deviations of the velocities, and visually from the high speed videos. Looking at Figure 4, the slope of the plot changes at 330 °C and 360 °C for the 80° and 45° samples, respectively. To the left of these temperatures the standard deviations are significantly larger. This indicates that the intermittent contact is occurring and the droplet is not in a stable film boiling state. Because this intermittent contact promotes an explosive type of energy transfer, it results in a wide range of droplet velocities and thus larger standard deviations. Figure 5 shows droplets at different locations and at temperatures near the Leidenfrost transition temperature for both samples. It can be seen from these images that there is a distinct visual difference between the two temperatures. For both samples, the droplets appear to be white in color and not very spherical at temperatures below the Leidenfrost temperature. This indicates that the droplet is being disturbed by the intermittent contact. At these temperatures, it can also be seen from the high speed video that the droplet tends to jump and bounce much more frequently and eject smaller satellite drops. This is characteristic of not having a fully developed vapor film and thus not in the Leidenfrost region. At temperatures above the Leidenfrost

temperature, the droplets appear very spherical and clear in color. This is due to the stable vapor film below the droplet.

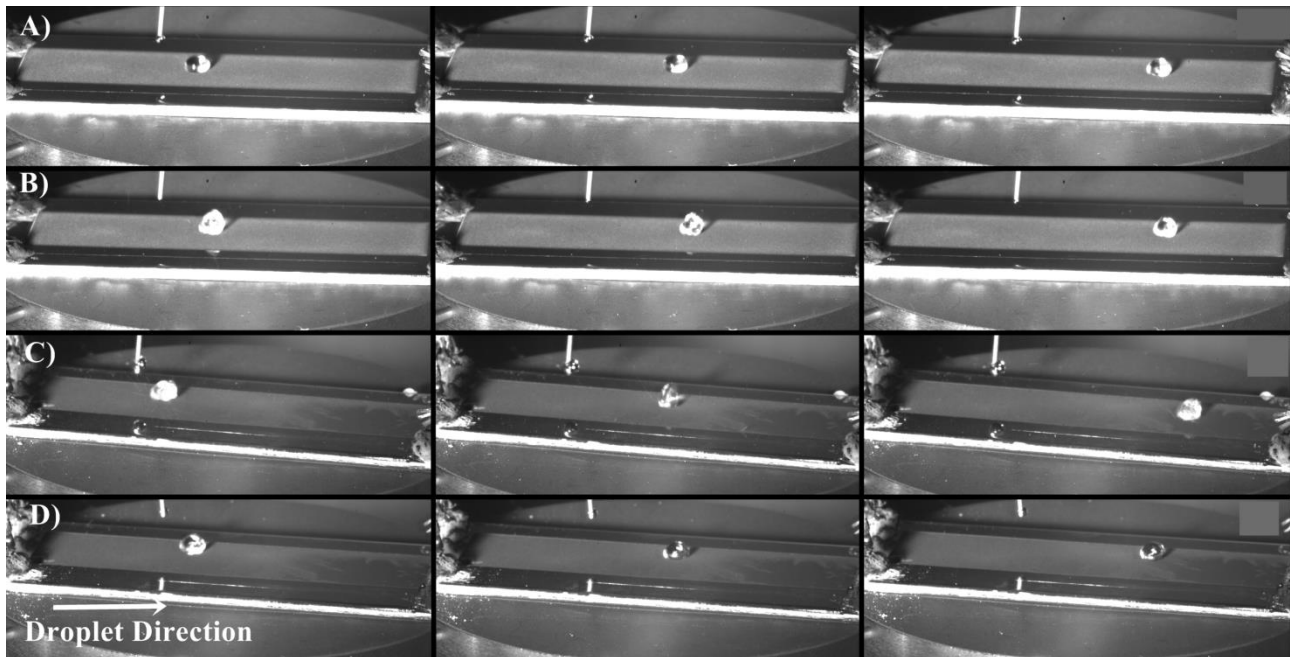


Fig. 5 Droplets at various positions along the sample at temperatures above and below the corresponding Leidenfrost temperature. A) 80° sample at 330 °C, B) 80 ° sample at 320 °C, C) 45° sample 340 °C, D) 45° sample 360 °C

4. SELF-PROPULSION MECHANISM

One of the most interesting aspects of the droplet motion found with our fish scale structures is that the direction of the droplets is opposite of conventional ratchet microstructures. The direction of the droplet motion with respect to the microstructure is explained in Figure 6. The mechanism that is widely used to describe the motion of the droplet is the viscous mechanism [14]. This mechanism explains that the vapor generated from the droplet evaporation is preferentially directed by the microstructures and as this vapor moves away from the droplet it drags the droplet with it due to viscous stresses. It has been shown experimentally that the vapor from a droplet flows in the direction of descending slope on the teeth of a ratchet (x -direction). When the flow encounters the next ratchet, the flow is redirected 90° (y -direction) and flows down the ratchet channels [14]. This flow is symmetric in the y direction and thus any forces due to this flow are canceled out. This leaves a net force in the x direction and thus results in the direction of the droplet. This also means that each of the ratchet segments is cellular and develops a similar, yet independent flow and force.

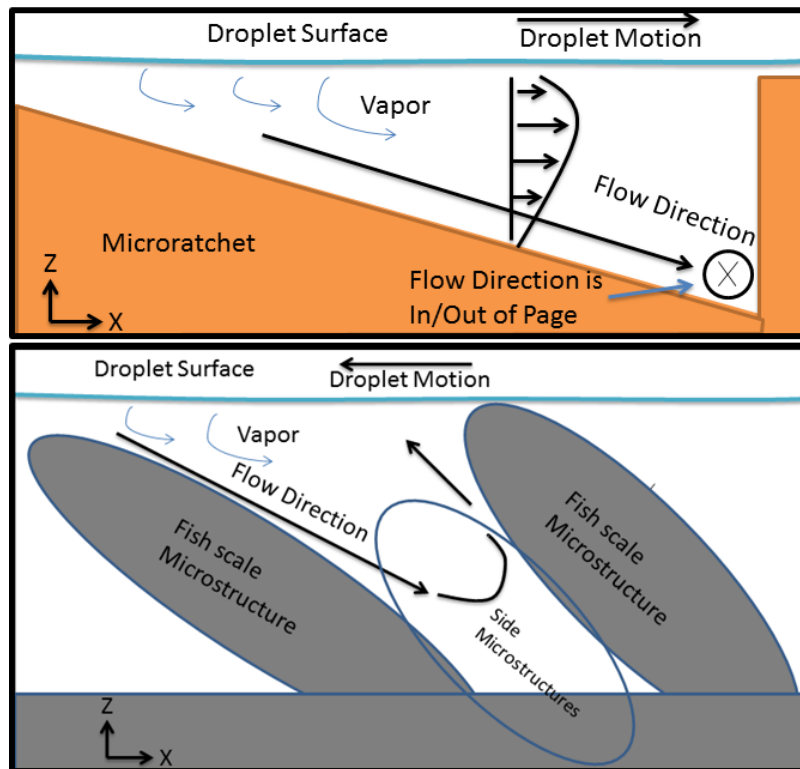


Fig. 6 Top: Shows the schematic for the flow direction and resulting droplet motion direction for a conventional ratchet microstructure. Bottom: Shows the flow direction and resulting droplet motion for the FLSP fish scale microstructure.

In principal, the viscous mechanism must also apply to our laser processed fish scale microstructures. But this theory does not fully describe why the droplet motion on these samples is in the opposite direction as the ratchet structures. If the fish scale microstructures are simplified to their simplest form, they are similar to the ratchet microstructures, however with one major difference. Because the fish scale structures are three dimensional and self-organized, this results in no clear channel in the y direction like with the ratchet structures. This difference is key to understanding why the direction of droplet motion is different between the two structures. When vapor is released from the droplet circumference, it initially follows a very similar profile as the ratchet structure. When this vapor reaches the bottom of the sloped region and encounters the next microstructure, the vapor cannot escape in the y direction like for the ratchet structure. The vapor is forced to be redirected nearly 180° . The redirected vapor drags the droplet with it through viscous stresses and causes the droplet to move in the opposite direction than that reported with the ratchet microstructures. Just like the ratchet structures, the fish scale structures are also cellular and independently result in a net force. Because the fish scale structures are three dimensional and self-organized, there may be vapor flow directions that oppose the overall droplet motion, but the dominant trend is to have a net force in the negative x direction. These opposing flow patterns could also be the reason why the maximum velocities seen in our data are lower than similar sized ratchet structures [17].

5. CONCLUSIONS

It has been shown in our work that fish scale microstructures created through the use of femtosecond laser surface processing can be used to effectively propel liquid droplets in the Leidenfrost state across a heated surface. The surface structures are characterized by a mound type structure with a rounded top that leans at a specific angle. These structures can be created at nearly any inclination angle. For this experiment two surfaces

were created with angles of 45° and 80° with respect to the horizontal. These two surfaces resulted in maximum velocities of 12.5 cm/s and 17.8 cm/s for the 80° and 45° samples. These maximum velocities occurred at temperatures slightly below the Leidenfrost temperature of the surface. The high velocities at temperatures below the Leidenfrost temperature of the surface are due to intermittent contact of the liquid droplet with the surface microstructures. When this occurs more energy is transferred to the droplet and vapor is violently ejected from the droplet. This vapor is preferentially directed by the microstructures into one general direction. Through viscous stress forces, the droplet is dragged in the direction of the net vapor flow. With respect to conventional ratchet structures, the fish scale structures result in droplet motion in the opposite direction. This change in the direction of the droplet motion is due to the three dimensional self-organized nature of the fish scale microstructures which leads to a redirection of the vapor flow and thus an opposite droplet direction. Further research is needed to fully understand the flow dynamics beneath the droplet, as well as the velocity dependencies on microstructure angle and droplet size.

ACKNOWLEDGMENT

This work has been supported by a grant through the Nebraska Center for Energy Sciences Research (NCSR) with funds provided by Nebraska Public Power District (NPPD) to the University of Nebraska – Lincoln (UNL) No. 4200000844, by funds from the Air Force Research Laboratory (AFRL) High Energy Laser-Joint Technology Office (HEL-JTO) No. FA9451-12-D-019/0001, JTO Number: 12-BAA-0467, and by funds from the Department of Mechanical and Materials Engineering and the College of Engineering at UNL, awarded to S.N.

REFERENCES

- [1] Chaudhury M., and Whitesides G., “How to make water run uphill,” *HARVARD UNIV CAMBRIDGE MA DEPT Chem.*(1992).
- [2] Brochard F., “Motions of droplets on solid surfaces induced by chemical or thermal gradients,” *Langmuir*, (3), pp. 432–438, (1989).
- [3] Brzoska J., Brochard-Wyart F., and Rondelez F., “Motions of droplets on hydrophobic model surfaces induced by thermal gradients,” *Langmuir*, pp. 2220–2224, (1993).
- [4] Santos F. Dos, and Ondarcuhu T., “Free-running droplets,” *Phys. Rev. Lett.*, 75(16)(1995).
- [5] John K., Bär M., and Thiele U., “Self-propelled running droplets on solid substrates driven by chemical reactions,” *Eur. Phys. J. E. Soft Matter*, 18(2), pp. 183–99, (2005).
- [6] Darhuber A. a., Valentino J. P., Davis J. M., Troian S. M., and Wagner S., “Microfluidic actuation by modulation of surface stresses,” *Appl. Phys. Lett.*, 82(4), p. 657, (2003).
- [7] Piroird K., Clanet C., and Quéré D., “Magnetic control of Leidenfrost drops,” *Phys. Rev. E*, 85(5), pp. 10–13, (2012).
- [8] Zhang, S., Gogos G., “Film evaporation of a spherical droplet over a hot surface: fluid mechanics and heat/mass transfer analysis,” *J. Fluid Mech.*, 222, pp. 543–563, (1991).
- [9] Biance A.-L., Clanet C., and Quéré D., “Leidenfrost drops,” *Phys. Fluids*, 15(6), p. 1632, (2003).
- [10] Burton J., Sharpe a., van der Veen R., Franco a., and Nagel S., “Geometry of the Vapor Layer Under a Leidenfrost Drop,” *Phys. Rev. Lett.*, 109(7), pp. 1–4, (2012).
- [11] Vakarelski I. U., Patankar N. a, Marston J. O., Chan D. Y. C., and Thoroddsen S. T., “Stabilization of Leidenfrost vapour layer by textured superhydrophobic surfaces,” *Nature*, 489(7415), pp. 274–7, (2012).
- [12] Linke H., Alemán B., Melling L., Taormina M., Francis M., Dow-Hygelund C., Narayanan V., Taylor R., and Stout a., “Self-Propelled Leidenfrost Droplets,” *Phys. Rev. Lett.*, 96(15), pp. 2–5, (2006).
- [13] Grounds A., Still R., and Takashina K., “Enhanced droplet control by transition boiling,” *Sci. Rep.*, 2(c), p. 720, (2012).
- [14] Dupeux G., Le Merrer M., Lagubeau G., Clanet C., Hardt S., and Quéré D., “Viscous mechanism for Leidenfrost propulsion on a ratchet,” *EPL (Europhysics Lett.)*, 96(5), p. 58001, (2011).
- [15] Hashmi A., Xu Y., Coder B., Osborne P. a, Spafford J., Michael G. E., Yu G., and Xu J., “Leidenfrost levitation: beyond droplets,” *Sci. Rep.*, 2, p. 797, (2012).
- [16] Lagubeau G., Le Merrer M., Clanet C., and Quéré D., “Leidenfrost on a ratchet,” *Nat. Phys.*, 7(5), pp. 395–398, (2011).
- [17] Ok J. T., Lopez-Oña E., Nikitopoulos D. E., Wong H., and Park S., “Propulsion of droplets on micro- and sub-micron ratchet surfaces in the Leidenfrost temperature regime,” *Microfluid. Nanofluidics*, 10(5), pp. 1045–1054, (2010).
- [18] Marin A. G., and Cerro D. A. del, “Capillary droplets on Leidenfrost micro-ratchets,” *Phys.*, pp. 1–9, (2012).
- [19] Bizi-Bandoki P., Benayoun S., Valette S., Beaugiraud B., and Audouard E., “Modifications of roughness and wettability properties of metals induced by femtosecond laser treatment,” *Appl. Surf. Sci.*, 257(12), pp. 5213–5218, (2011).

- [20] Wang Z. K., Zheng H. Y., and Xia H. M., "Femtosecond laser-induced modification of surface wettability of PMMA for fluid separation in microchannels," *Microfluid. Nanofluidics*, 10(1), pp. 225–229, (2010).
- [21] Wu J., Xia J., Lei W., and Wang B., "A one-step method to fabricate lotus leaves-like ZnO film," *Mater. Lett.*, 65(3), pp. 477–479, (2011).
- [22] Baldacchini T., Carey J. E., Zhou M., and Mazur E., "Superhydrophobic surfaces prepared by microstructuring of silicon using a femtosecond laser," *Langmuir*, 22(11), pp. 4917–9, (2006).
- [23] Crouch C. H., Carey J. E., Warrender J. M., Aziz M. J., Mazur E., and Génin F. Y., "Comparison of structure and properties of femtosecond and nanosecond laser-structured silicon," *Appl. Phys. Lett.*, 84(11), p. 1850, (2004).
- [24] Dolgaev S. I., Lavrishev S. V., Lyalin a. a., Simakin a. V., Voronov V. V., and Shafeev G. a., "Formation of conical microstructures upon laser evaporation of solids," *Appl. Phys. A Mater. Sci. Process.*, 73(2), pp. 177–181, (2001).
- [25] Koch K., Bhushan B., Jung Y. C., and Barthlott W., "Fabrication of artificial Lotus leaves and significance of hierarchical structure for superhydrophobicity and low adhesion," *Soft Matter*, 5(7), p. 1386, (2009).
- [26] Stratakis E., Ranella a, and Fotakis C., "Biomimetic micro/nanostructured functional surfaces for microfluidic and tissue engineering applications," *Biomicrofluidics*, 5(1), p. 13411, (2011).
- [27] Feng L., Zhang Y., Xi J., Zhu Y., Wang N., Xia F., and Jiang L., "Petal effect: a superhydrophobic state with high adhesive force," *Langmuir*, 24(8), pp. 4114–9, (2008).
- [28] Kruse C., Anderson T., Wilson C., Zuhlke C., Alexander D., Gogos G., and Ndao S., "Extraordinary shifts of the Leidenfrost temperature from multiscale micro/nanostructured surfaces," *Langmuir*, 29(31), pp. 9798–806, (2013).
- [29] Tull B., Carey J., and Mazur E., "Silicon surface morphologies after femtosecond laser irradiation," *Mrs ...*, 31(August), pp. 626–633, (2006).
- [30] Wu B., Zhou M., Li J., Ye X., Li G., and Cai L., "Superhydrophobic surfaces fabricated by microstructuring of stainless steel using a femtosecond laser," *Appl. Surf. Sci.*, 256(1), pp. 61–66, (2009).
- [31] Nayak B. K., Gupta M. C., and Kolasinski K. W., "Spontaneous formation of nanospiked microstructures in germanium by femtosecond laser irradiation," *Nanotechnology*, 18(19), p. 195302, (2007).
- [32] Nayak B. K., and Gupta M. C., "Ultrafast laser-induced self-organized conical micro/nano surface structures and their origin," *Opt. Lasers Eng.*, 48(10), pp. 966–973, (2010).
- [33] Her T.-H., Finlay R. J., Wu C., and Mazur E., "Femtosecond laser-induced formation of spikes on silicon," *Appl. Phys. A Mater. Sci. Process.*, 70(4), pp. 383–385, (2000).
- [34] Yong Hwang T., and Guo C., "Polarization and angular effects of femtosecond laser-induced conical microstructures on Ni," *J. Appl. Phys.*, 111(8), p. 083518, (2012).
- [35] Vorobyev A. Y., and Guo C., "Direct femtosecond laser surface nano/microstructuring and its applications," *Laser Photon. Rev.*, 7(3), pp. 385–407, (2013).
- [36] Zuhlke C., Anderson T., and Alexander D., "Formation of multiscale surface structures on nickel via above surface growth and below surface growth mechanisms using femtosecond laser pulses," *Opt. Express*, 21(7), pp. 97–98, (2013).
- [37] Bradfield W., "Liquid-solid contact in stable film boiling," *Ind. Eng. Chem. Fundam.*(1966).
- [38] Kim H., Truong B., Buongiorno J., and Hu L.-W., "On the effect of surface roughness height, wettability, and nanoporosity on Leidenfrost phenomena," *Appl. Phys. Lett.*, 98(8), p. 083121, (2011).